FERMILAB-PUB-19-052-TD
ACCEPTED

Summary of the Mechanical Performances of the 1.5 m Long Models of the Nb_3Sn Low-β Quadrupole MQXF

G. Vallone, G. Ambrosio, E. Anderssen, H. Bajas, N. Bourcey, D. W. Cheng, G. Chlachidze, P. Ferracin, P. Grosclaude, M. Guinchard, S. Izquierdo Bermudez, M. Juchno, H. Pan, J.C. Perez, S. Prestemon, T. Strauss

***Abstract*—The Nb_3Sn quadrupole MQXF is being developed as a part of the LHC High Luminosity upgrade. The magnet design was tested on 1.5 m long short models, sharing the same cross-section with the full-length magnets. Various azimuthal and longitudinal preloads were applied, studying the impact on the magnet training and on its mechanical performances. The experiments demonstrated the possibility to control the magnet prestress. However, various factors, coil size among the others, may affect the stress variation between and within each winding. This variation could prevent the magnet to reach the desired performances, for example as result of critical current degradation of the Nb_3Sn strands. This paper analyzes the mechanical performances of the short models, studying in particular the stress variation on different coils. The measured coil size was used as input in the numerical simulations, and results were then compared with the strain gauge measurements. Finally, the short models experience was used to evaluate the feasibility of a loading operation that does not rely on the strain measurements.**

***Index Terms*—High Luminosity LHC, Low-β Quadrupole, Nb3Sn magnet, Mechanical Performance, Short Model.**

I. Introduction

THE Nb_3Sn quadrupole MQXF will be installed in the LHC triplets as a part of the High Luminosity upgrade [1]. The magnet will be produced in two different magnetic lengths, 4.2 m (MQXFA) and 7.15 m (MQXFB), aiming for an ultimate gradient of $143.2\,\mathrm{T/m}$ in a $150\,\mathrm{mm}$ aperture, at an ultimate current of $17.89\,\mathrm{kA}$ [2]. Up to this moment, 4 short models, with a magnetic length of $1.2\,\mathrm{m}$, were tested: MQXFS1, MQXFS3, MQXFS5 and MQXFS4. The models share the same cross-section, shown in Fig. 1, with the accelerator magnets. The mechanical performance of the structure was monitored during assembly, cooldown and powering by means of electrical strain gauges, installed on the aluminum shells and on the winding poles [3].

Automatically generated dates of receipt and acceptance will be placed here
This work was supported by the High Luminosity LHC Project at CERN and by the DOE through the U.S. LHC Accelerator Research Program.

G. Vallone, E. Anderssen, D. W. Cheng, M. Juchno, H. Pan and S. Prestemon are with Lawrence Berkeley National Laboratory, Berkeley, CA 94720 USA (e-mail: gvallone@lbl.gov).

G. Ambrosio, G. Chlachidze and T. Strauss are with the Fermi National Accelerator Laboratory, Batavia, IL 80510 USA.

H. Bajas, N. Bourcey, P. Ferracin, P. Grosclaude, M. Guinchard, S. Izquierdo Bermudez and J.C. Perez are with the European Organization for Nuclear Research (CERN), 1211 Geneva, Switzerland.

Colour versions of one or more of the figures in this paper are available online at http://ieeexplore.ieee.org.
Digital Object Identifier: xx

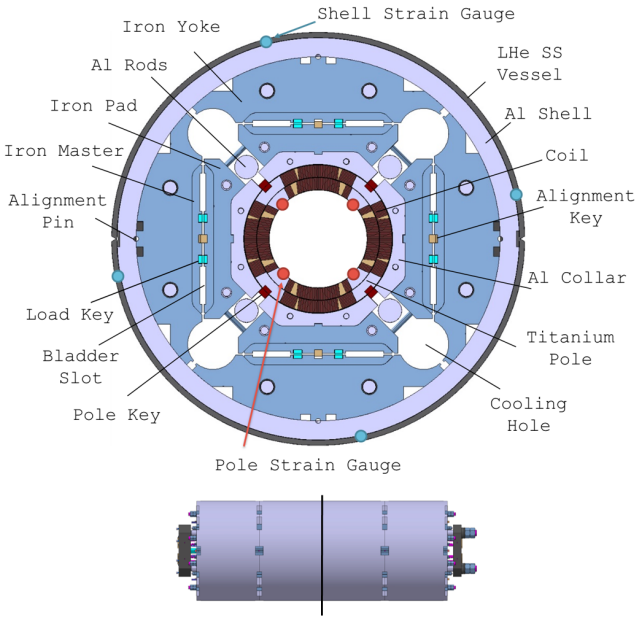

Fig. 1. MQXF cross-section (top), and longitudinal view of the short models (bottom). The strain gauges were installed on the shell and the winding poles, as shown by the circular markers. The vertical line in the bottom view provides their longitudinal position.

The MQXF design allows to apply a controlled azimuthal prestress at room temperature by means of the bladder and key technology [4]. The longitudinal prestress is instead provided by longitudinal rods, pretensioned by means of an hydraulic piston and locked in this deformed state with bolts. The differential thermal contraction of the various components increases both the azimuthal and longitudinal prestress during the magnet cooldown at cryogenic temperature. A more detailed description of the magnet mechanics can be found in [3], [5].

II. MQXF Short Model Magnets

Training curve and mechanical performance of the first 3 short models (MQXFS1, MQXFS3 and MQXFS5) were presented in [3], [6]. A summary of all the training curves for the tested models is provided in 2. The corresponding prestress levels applied are shown in Fig. 3. The MQXFS3 magnet was tested with two different longitudinal prestresses, as MQXFS3a and MQXFS3b. In both cases the magnet failed

This manuscript has been authored by Fermi Research Alliance, LLC under Contract No. DE-AC02-07CH11359 with the U.S. Department of Energy, Office of Science, Office of High Energy Physics.

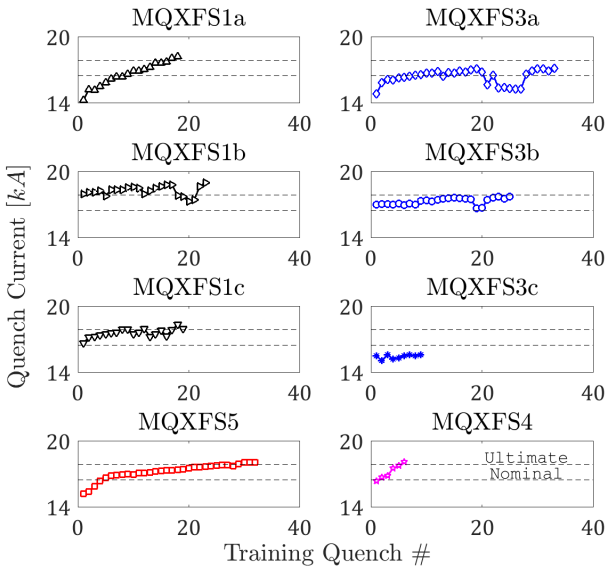

Fig. 2. Quench currents at 20 A/s for all the short models tested. The best training performances were reached by the last magnet tested, MQXFS4, that reached the ultimate current in 6 quenches.

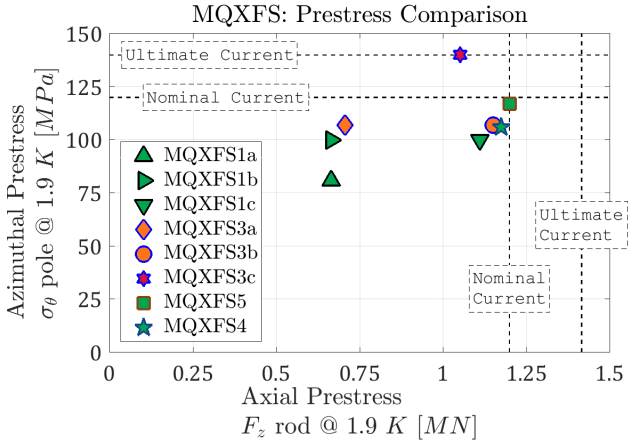

Fig. 3. Summary of the applied prestress in all the MQXF short models tested up to now. The horizontal axis describes the amount of longitudinal prestress applied, the vertical axis the azimuthal one. The vertical and horizontal line describe the prestress values required to avoid possible unloading of the coilx during powering at nominal and ultimate current. The markers are filled in green, orange or red to indicate magnets that reached a maximum quench current higher than ultimate, nominal or lower than nominal.

to reach the ultimate current. The increased prestress produced, however, some beneficial effects on the magnet performance [7]. The degraded quenches were all localized in one coil, that was subsequently swapped.

The magnet was then tested again as MQXFS3c, with the highest azimuthal prestress applied in all the short models, equal to 140 MPa. The relationship between the shell and pole azimuthal stresses (prestress transfer function [3]) is showed in Fig. 4. To reach this stress level while avoiding any damage on the structure, it is necessary to leave a gap between the alignment pole key and the collar sides. This strategy was already adopted in the MQXFS5 magnet, where a total gap of 200 µm was left, and discussed in detail in

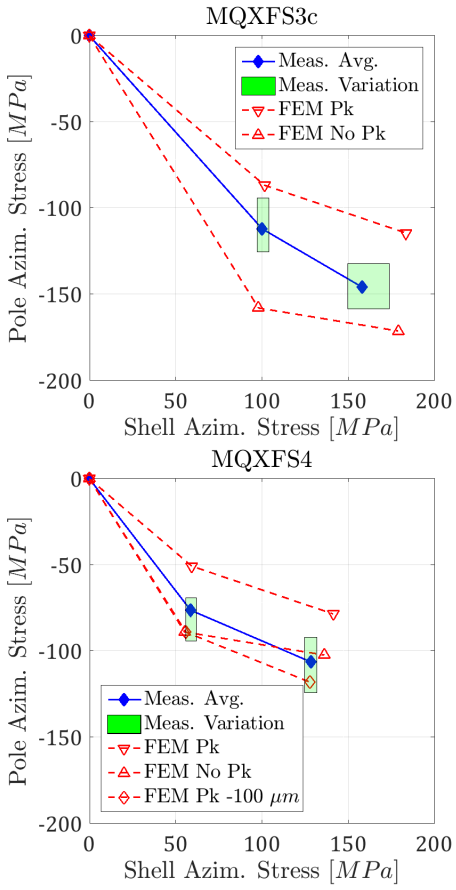

Fig. 4. Prestress transfer function for MQXFS3c (top) and MQXFS4 (bottom). Red dashed lines provide the FE model computations, blue continuous lines the measured average, and the green boxes the variation across the four quadrants. Both magnets were loaded with a clearance between the alignment pole key and the collars.

[6]. In this case, given the higher prestress target, a bigger gap of 400 µm was left. The measured longitudinal prestress at 1.9 K was equal to 1.05 MN. The magnet failed again to reach the desired performances whit the nominal ramp rate of 20 A s. Nevertheless, the ultimate current was reached when powering at 200 A s [8]. The limiting quenches were in a location similar to the one that limited the MQXFS3a and MQXFS3b magnets, in a coil that was already tested in these past experiments. As a consequence, it was not possible to conclude if the poor performances were due to the higher prestress applied or to a damage that was possibly already initiated by the previous experiments. The evolution of the azimuthal stress during magnet powering is shown in Fig. 5. The stress measured on the winding pole does not show unloading [9] up to the ultimate current. The test demonstrated that the MQXF structure can provide the prestress required to avoid unloading up to the ultimate current.

For the last magnet tested, MQXFS4, the prestress target was defined to be the MQXFS5 one, an intermediate level that is the target for the series. As a consequence, the same alignment key gap, 200 µm was left. The transfer function is shown in Fig. 4. The measured azimuthal prestress after cool-down was equal to 106 MPa. This is 11 MPa lower

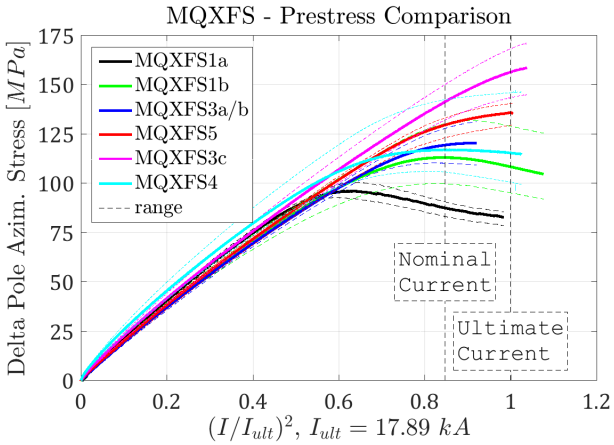

Fig. 5. Evolution of the pole azimuthal stress as a function of the applied e.m. forces. The MQXFS3c magnet did not show unloading up to the ultimate current. MQXFS5 and MQXFS4 magnets unload close to the nominal current.

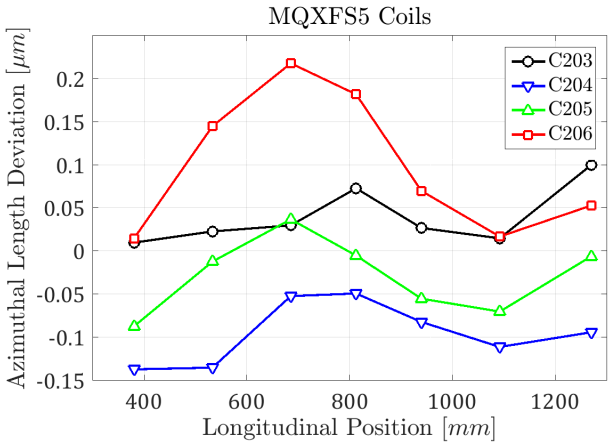

Fig. 6. MQXFS5 coil size along the length. The size deviations from the average are generally contained within ±100 μm.

TABLE I
IMPACT OF A 100 μm COIL SIZE INCREASE ON THE COIL STRESSES, MPA

	Al. Shell†	Pole†	Coil-Pole‡	Mid-Plane‡
R.T. Loading	5	-21	-12	-10
Cool-down	6	-20	-12	-10
Ultimate current	6	-25	-13	-10

† Strain gauge location, see Fig. 1.
‡ Mid-radius.

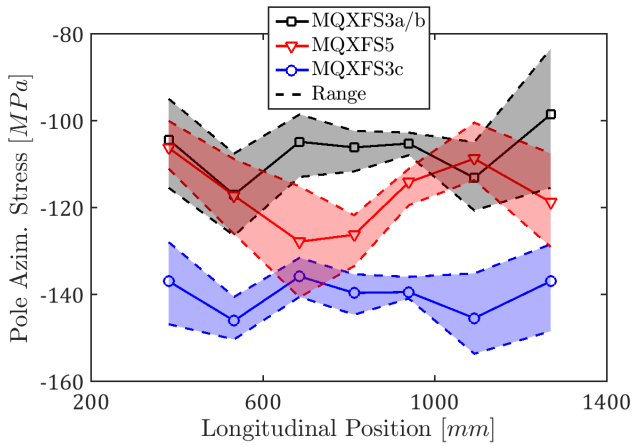

Fig. 7. Azimuthal prestress variation along the straight section. The results are computed on the basis of the measured size of the coils, using the FE approach. The computed stress variation is within ±20 MPa in all the magnets.

than the target MQXFS5 prestress, equal to 117 MPa. This small discrepancy was not due to an imprecision in the estimation of the stress increase during cooldown. In fact, as evident from Fig. 4, the experimental values matched perfectly the prediction. Rather, to a conservative choice during the assembly operation. The longitudinal prestress was equal to 1.17 MN, very close to the target, 1.20 MN. The magnet reached the ultimate current in only 6 quenches, becoming the best performing short models. This improved performance with respect to the MQXFS5 magnet could be due to the better critical current density of the conductor [10]. The magnet showed signs of unloading close to the nominal current (Fig. 5).

III. AZIMUTHAL PRESTRESS VARIATION

The pole and shell stresses were measured only in the central section of the short models, as shown in Fig. 1. However, the real stress applied in each section could vary as a function of the coil size. An estimation of the coil stress variation $\Delta\sigma$ can be obtained assuming that the coils will have to compensate for their imperfect size deforming in an infinitely rigid structure:

$$\Delta\sigma = E_t \frac{2\Delta(L+R)}{\pi R_m} \quad (1)$$

where $\Delta(L+R)$ is the local azimuthal oversize [11], R_m is the average radius of the coil, and E_t is the average modulus of the coil. This modulus can be estimated considering the coil as a system of springs: the inner layer and outer layer components are considered in series, and the two layers in parallel. With these simplifications the computed modulus E_t is equal to 40 GPa. The impact of a 100 μm size increase is then equal to 27 MPa. Because of the assumption of a completely rigid structure, this has to be considered the upper limit of the size variation sensitivity for a MQXF coil.

A more precise estimate was obtained from finite element models. The increased coil size was introduced as a variation of the outer radius of the coil, manipulating the contact conditions at the collars interface. The impact on the coil stresses for a 100 μm size increase of the coil is reported in Table I: the prestress variation after cooldown is equal to 20 MPa at the winding pole, representative of the coil stress at the inner radius of the coil-pole interface, and also very close to the coil peak stress [3]. The coil deformation is affected by a bending mode that compresses the inner radius. Because of this, a smaller stress variation is seen by the coil at the mid-radius, equal to 12 MPa at the pole interface and 10 MPa at the mid-plane. The finite element computation produced a smaller variation than the one estimated using Eq. 1. This is because the structure is now absorbing part of the size variation, as also shown by the increase in the aluminum shell stress, equal

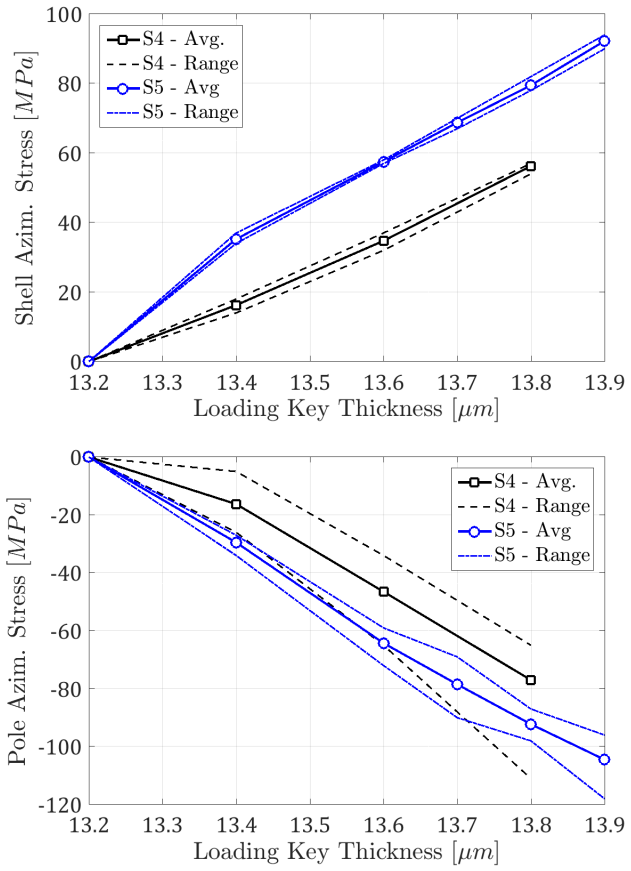

Fig. 8. Shell (top) and pole (bottom) measured azimuthal stress variation during room temperature loading, as a function of the loading key thickness.

to 6 MPa.

This sensitivity value was then used to compute the local stresses on the basis of the coil azimuthal size deviations. An example of the size distribution along the length is provided for the MQXFS5 magnet in Fig. 6. The average deviation of the coil from the nominal size can be neglected, being already corrected by means of polyamide shims applied on the mid-plane and on the outer radius [12]. As a consequence, the only relevant number is the local coil size deviation from the same coil average size. The impact of this size variation can be found using the sensitivity study results from Table I. Finally, the local winding pole stress can be estimated summing its variation to the measured average stress. The resulting stress variation along the magnet length is shown in Fig. 7. With a coil size variation generally within ± 100 µm [11], the azimuthal stress at the winding pole is always in a range of ± 20 MPa. This variation is very close to the one that was measured in the short models [3], [6].

IV. Azimuthal Prestress Control

The loading operation of the short models relied heavily on the readings from the strain gauges. The azimuthal prestress operation consisted in the insertion of loading keys of increasing thickness, up to a target value of the pole measured azimuthal stress. However, on the full length magnets, the installation of strain gauges on the winding poles could be unfeasible due to the presence of the cold bore. The current plan is to install Fiber Bragg Grating sensors, as already tested on MQXFS5 [13]. An alternative would be to monitor only the shell stress. The shell stress required to reach a certain amount of pole stress is mainly governed by the amount of force that is intercepted by the pole alignment key. This allows to control the force demanded to the structure to produce a certain pole stress. On the other hand, it also introduces an uncertainty in the pole stress for a given shell stress [6]. It is then interesting to evaluate the feasibility of controlling the prestress defining a standard loading key thickness.

Fig. 8 shows the relationship between the loading key thickness and the shell and pole azimuthal stresses, as measured on MQXFS4 and MQXFS5, two magnets that had the same pole key gap. The MQXFS4 magnet showed an initial nonlinearity, with a lower increase of the stress for the same key thickness increase. This could be due either to an imperfect contact of the coils to the collars [14], or to a reduced radial dimension of the coil pack. The latter hypothesis is consistent with the reduced amount of radial shimming used in MQXFS4. In particular, in MQXFS5 a 125 µm radial distance between the shimmed coils and the nominal position of the collars was left. In MQXFS4 a distance of 250 µm was left, in an attempt of improving the coil-collar contact [14]. After this initial phase, the stress undergoes similar increases in both magnets, with a slight slope decrease in MQXFS5, a signal that the pole key is going in contact with the collar sides. With a loading key 13.8 mm thick, the average stress difference is 15 MPa. Further experiments are required to understand if this result is repeatable or not, and if consistent radial shimming strategies could close the gap between the magnets.

V. Conclusion

This paper summarizes the mechanical performances of the latest MQXF short models: MQXFS3c and MQXFS4. The structure demonstrated the capability to apply prestresses up to the ultimate current. However, this high prestress value was applied only on the MQXFS3c magnet, which did not reach the desired performances. The available data does not allow to conclude if the magnet degradation was a consequence of the high prestress applied. The MQXFS4 magnet loading parameters were set as close as possible to MQXFS5. The loading operation was however conservatively stopped earlier, giving a final prestress 11 MPa lower.

The influence of the coil size deviation on the actual stress in the sections where the stress is not measured was investigated. The stress variation was estimated analytically to be ± 27 MPa, and ± 20 MPa using a finite element model.

Finally, the authors evaluated the possibility to estimate the actual prestress applied on the basis of the sole loading key thickness. The MQXFS4 and MQXFS5 experiments show a difference of 15 MPa for the same key thickness of 13.8 mm. This is lower than the usual stress variation measured between different coils.

REFERENCES

[1] L. Rossi and O. Brüning, "High Luminosity Large Hadron Collider: a description for the European Strategy Preparatory Group," CERN, Geneva, Swtizerland, CERN-ATS-2012-236, 2012.

[2] P. Ferracin *et al.*, "Development of MQXF: The Nb_3Sn low-β quadrupole for the HiLumi LHC," *IEEE Transactions on Applied Superconductivity*, vol. 26, no. 4, pp. 1–7, 2016.

[3] G. Vallone *et al.*, "Mechanical performance of short models for MQXF, the Nb_3Sn low-β quadrupole for the Hi-Lumi LHC," *IEEE Transactions on Applied Superconductivity*, pp. 1–5, 2016.

[4] S. Caspi *et al.*, "The use of pressurized bladders for stress control of superconducting magnets," *IEEE Transactions on Applied Superconductivity*, vol. 11, no. 1 II, pp. 2272–2275, 2001.

[5] M. Juchno *et al.*, "Mechanical Qualification of the Support Structure for MQXF, the Nb3Sn Low-β quadrupole for the high luminosity LHC," *IEEE Transactions on Applied Superconductivity*, vol. 26, no. 4, 2016.

[6] G. Vallone *et al.*, "Mechanical analysis of the short model magnets for the Nb_3Sn low-β quadrupole mqxf," *IEEE Transactions on Applied Superconductivity*, vol. 28, no. 3, pp. 1–6, 2018.

[7] H. Bajas *et al.*, "Test result of the short models MQXFS3 and MQXFS5 for the HL-LHC upgrade," *IEEE Transactions on Applied Superconductivity*, vol. 28, no. 3, pp. 1–6, 2018.

[8] F. J. Mangiarotti *et al.*, "To be defined," *IEEE Transactions on Applied Superconductivity*, 2018, Under Review.

[9] G. Vallone and P. Ferracin, "Modeling coil-pole debonding in Nb_3Sn superconducting magnets for particle accelerators," *IEEE Transactions on Applied Superconductivity*, 2017.

[10] P. Ferracin *et al.*, "The HL-LHC low-β quadrupole magnet MQXF: from short models to long prototypes," *IEEE Transactions on Applied Superconductivity*, 2018, Under Review.

[11] J. F. Troitino *et al.*, "Applied metrology in the production of superconducting model magnets for particle accelerators," *IEEE Transactions on Applied Superconductivity*, vol. 28, no. 3, pp. 1–6, 2018.

[12] H. Pan *et al.*, "Assembly tests of the first Nb_3Sn low-β quadrupole short model for the Hi-Lumi LHC," *IEEE Transactions on Applied Superconductivity*, vol. 26, no. 4, pp. 1–5, Jun. 2016.

[13] A. Chiuchiolo *et al.*, "Strain measurements with fiber bragg grating sensors in the short models of the hilumi lhc low-β quadrupole magnet MQXF," *IEEE Transactions on Applied Superconductivity*, 2018.

[14] P. Ferracin *et al.*, "Mechanical performance of the LARP Nb_3Sn quadrupole magnet LQS01," *IEEE Transactions on Applied Superconductivity*, vol. 21, no. 3, pp. 1683–1687, Jun. 2011.